

The WARPS survey – IV: The X-ray luminosity–temperature relation of high redshift galaxy clusters

B. W. Fairley^{1,8}, L. R. Jones¹, C. Scharf², H. Ebeling³, E. Perlman²,
D. Horner^{4,7}, G. Wegner⁵ and M. Malkan⁶

¹ School of Physics and Astronomy, University of Birmingham, Birmingham, B15 2TT, UK

² Space Telescope Science Institute, Baltimore, MD 21218, USA

³ Institute for Astronomy, 2680 Woodlawn Dr, Honolulu, HI 96822, USA

⁴ Laboratory for High Energy Astrophysics, Code 660, NASA/GSFC, Greenbelt, MD 20771, USA

⁵ Dept. of Physics & Astronomy, Dartmouth College, 6127 Wilder Lab., Hanover, NH 03755, USA

⁶ Dept. of Astronomy, UCLA, Los Angeles, CA 90024, USA

⁷ University of Maryland, College Park, MD 20742-2421, USA

⁸ Email: bwf@star.sr.bham.ac.uk

Accepted; Received; in original form

ABSTRACT

We present a measurement of the cluster X-ray luminosity-temperature relation out to high redshift ($z \sim 0.8$). Combined *ROSAT* PSPC spectra of 91 galaxy clusters detected in the Wide Angle *ROSAT* Pointed Survey (WARPS) are simultaneously fit in redshift and luminosity bins. The resulting temperature and luminosity measurements of these bins, which occupy a region of the high redshift L-T relation not previously sampled, are compared to existing measurements at low redshift in order to constrain the evolution of the L-T relation. We find a best fit to low redshift ($z < 0.2$) cluster data, at $T > 1$ keV, to be $L \propto T^{3.15 \pm 0.06}$. Our data are consistent with no evolution in the normalisation of the L-T relation up to $z \sim 0.8$. Combining our results with *ASCA* measurements taken from the literature, we find $\eta = 0.19 \pm 0.38$ (for $\Omega_0 = 1$, with 1σ errors) where $L_{\text{Bol}} \propto (1+z)^\eta T^{3.15}$, or $\eta = 0.60 \pm 0.38$ for $\Omega_0 = 0.3$. This lack of evolution is considered in terms of the entropy-driven evolution of clusters. Further implications for cosmological constraints are also discussed.

Key words: galaxies: clusters: general – methods: data analysis – surveys – X-rays: galaxies – cosmology: observations

1 INTRODUCTION

Clusters of galaxies, as the largest virialised objects in the Universe, allow us a unique insight into the formation and evolution of mass clustering on cosmological time-scales. The X-ray emission from galaxy clusters originates from hot ($T \sim 10^{7-8}$ K) intra-cluster gas which, in relaxed systems, is in hydrostatic equilibrium with the cluster’s total gravitational field. Since the temperature of the gas is proportional to its mass, the observed correlation between X-ray luminosities and temperatures implies a relationship between cluster baryon mass and total mass. Thus, studying the evolution of the L–T relation probes the interrelated evolution of these mass components. One of the first attempts at modelling these properties assumed self-similar evolution of

both the gravitational potential and the baryonic intracluster medium (ICM) at varying cosmological epochs (Kaiser 1986).

These self-similar predictions are in conflict with observational evidence. The strong positive evolution of the cluster X-ray luminosity function (XLF) originally predicted (assuming realistic cosmological parameters) is in stark contrast to the negative evolution reported by Gioia et al. (1990) and Henry et al. (1992) for X-ray luminous clusters. The prediction is also in conflict with the results of more recent cluster surveys which find no significant evolution, at any luminosity, out to moderate redshift ($z \sim 0.3$, Ebeling et al. 1997; De Grandi et al. 1999), and again no significant (or mild negative) evolution at low and intermediate luminosities and high redshifts (Rosati et al. 1995; Burke et al. 1997;

Vikhlinin et al. 1998a; Jones et al. 1998b). To account for such discrepancies, modifications were suggested to the self-similar theory. Kaiser (1991) and Evrard & Henry (1991) modelled a 'pre-heated ICM', in which an initial injection of energy broke the direct self-similar scaling by introducing an entropy floor in cluster cores. It also brought theoretical predictions of cluster properties into better agreement with observational constraints.

Tests of gravitational self-similar scaling are thus fundamental to the understanding of cluster evolution. One such test used in this analysis is the study of the cluster X-ray luminosity–temperature (L–T) relation, which was predicted by the original self-similar model to be described by an $L \propto T^2$ law. However, a relationship closer to $L \propto T^3$, has been found by several cluster surveys and compilations (e.g. Edge & Stewart 1991; David et al. 1993; White et al. 1997), whilst even further steepening of the relation is required to agree with galaxy group measurements (Ponman et al. 1996; Helsdon & Ponman 2000). In addition to predicting the slope of the L–T relation, self-similar theory also predicts significant evolution in the normalisation of this relation at different redshifts. However, the evolution predicted is reduced in low density cosmologies, or by significant entropy injection at early epochs (e.g. Kaiser 1991; Cen & Ostriker 1994; Kay & Bower 1999).

Attempts at constraining evolution in the L–T relation, at redshifts above $z \sim 0.1$, are complicated by the inherent difficulty of temperature estimation from often poor signal-to-noise data. Mushotzky & Scharf (1997), using *ASCA* data from a sample of 38 clusters at $z > 0.14$, found no significant evolution out to $z \sim 0.3$. Prior to this work, the only attempt at quantifying evolution of the L–T relation to $z \sim 0.3$ was that of Henry et al. (1994), whose results were also consistent with no evolution. Henry et al. (1994) used low signal-to-noise spectra of 67 clusters observed with the *Einstein* observatory, each individually spectrally fitted, and then averaged together in redshift bins. Recently Donahue et al. (1999) have used *ASCA* measurements of clusters drawn from the *Einstein* Medium Sensitivity Survey (EMSS, Gioia et al. 1990; Henry et al. 1992) to extend the conclusion of no evolution to $z > 0.5$.

In this paper we present an L–T relation based on *ROSAT* spectra of WARPS clusters, in various redshift and luminosity bins. Although this procedure is analogous to the one adopted by Henry et al. (1994), a more sophisticated simultaneous fitting method is adopted here. We discuss the data analysis techniques used to obtain temperature estimates from often low signal-to-noise *ROSAT* PSPC data, and present results from simulated spectra to demonstrate their validity. In order to allow self-consistent discussion of any evolutionary effects in our relation, we compare our results with a local L–T relation over a wide range of temperatures and luminosities.

2 SAMPLE SELECTION

Traditional studies of galaxy clusters have relied on optically selected cluster samples. Whilst these surveys were often large, they suffered from biasing caused by projection effects and erroneous identifications (Lucey 1983; Frenk et al. 1990; Struble & Rood 1991). The recent trend, therefore, has been

to base large cluster surveys on X-ray selection techniques. This takes advantage of the X-ray emission from diffuse gas, trapped in a cluster's gravitational potential well, representing direct evidence of a three-dimensionally bound system. Several recent serendipitous cluster surveys have been compiled, all based on archival *ROSAT* PSPC data (e.g. Castander et al. 1995; Rosati et al. 1995; Collins et al. 1997; Vikhlinin et al. 1998b; Romer et al. 2000).

The Wide Angle *ROSAT* Pointed Survey (WARPS, Scharf et al. 1997) is also based on archival *ROSAT* PSPC data. It is a serendipitous cluster survey which uses a sophisticated source detection algorithm, VTP (Ebeling & Wiedemann 1993), capable of detecting arbitrarily shaped emission, down to very low surface brightness levels. An extensive optical follow-up program then spectroscopically confirms the concordance of galactic redshifts within each candidate cluster (Jones et al. 1998a). When complete, the WARPS survey will have generated a statistically complete, flux-limited catalogue covering a solid angle of more than 73 deg² and including approximately 150 X-ray selected galaxy clusters.

The sample used in this paper comprises 91 clusters identified in the WARPS survey, with redshifts in the range from $z = 0.11$ to $z = 0.833$. The WARPS survey is flux-limited at 6×10^{-14} ergs⁻¹ cm⁻² (0.5–2 keV) in total cluster flux and is restricted to *ROSAT* pointings of more than 8-ks exposure at $|b| > 20$ deg. Only the most sensitive area of the PSPC detector, at off-axis angles of $3 < r < 15$ arcmin, is used. In addition to the archival *ROSAT* PSPC data, deep optical imaging of the clusters, optical spectroscopy of all the brightest cluster galaxies (BCGs) and in some cases *ROSAT* HRI data are available (Jones et al. 1998a; Perlman et al. 2000).

3 DATA REDUCTION

3.1 Spectral fitting

For this work, the archival *ROSAT* PSPC data, containing the 91 WARPS clusters selected, were initially reduced and analysed using the Starlink ASTERIX package (Allan & Vallance 1995). The data were screened to minimize particle background rates by restraining the Master Veto Rate housekeeping parameter to a range of 0 to 170. The Aspect Error and Accepted Event Rate parameters were also limited to ranges of 0 to 2 and 0 to 30 respectively. The observation time thus removed was on average 5 per cent. The resulting cleaned data were then used to produce binned spectral cubes, with one spectral and two spatial dimensions, from *ROSAT* channels 11 through 231, with energy ranges of 0.114 to 2.295 keV

Background subtraction for each field was achieved by creating a model background spectral cube. Firstly an annulus was selected between 9 and 15 arcmin off-axis. This area is included in the WARPS analysis and was selected to minimize vignetting extrapolation errors in the background model. The background cube was projected to an image and searched for point sources using the ASTERIX PSS algorithm. Removal of the sources resulted in a new background model. This process was iteratively repeated until no more point sources were detected. The point source free cube

was then further edited manually to eliminate any extended sources, such as cluster emission. The background level of this cube was then extrapolated over all off-axis angles, using the known energy-dependent vignetting behaviour of the detector, to produce a final background model.

After background subtraction, a spectrum of the cluster was obtained by projecting a selected area of the spectral cube on to the energy axis, before correcting for energy-dependent vignetting and exposure effects. The circular extraction regions around the clusters had initial radii of 700 and 900 kpc, for $z < 0.5$ and $z > 0.5$ respectively (we assumed $H_0 = 50 \text{ km s}^{-1} \text{ Mpc}^{-1}$ and $q_0 = 0$). These radii were manually re-selected, where required, to eliminate contamination from nearby non-cluster sources. A background spectrum from the same area of sky, obtained from the source-free background model, was then associated with the cluster spectrum to allow spectral fitting using the maximum-likelihood C -statistic (Cash 1979). The number of counts in the cluster spectra ranged from 25 to 1001 (0.11–2.3 keV) with a median value of ~ 120 counts. The signal-to-noise ratios of the data varied dramatically, depending primarily on background level, exposure time and extraction radius. The average signal-to-noise level was ~ 6.8 in the 0.1–2.3 keV band, but was significantly higher in the 0.5–2 keV band used in the initial detection (Scharf et al. 1997). Thus C -statistic fitting was selected to avoid biases inherent in χ^2 fitting for low count-per-bin data (Nousek & Shue 1989).

The spectral models fitted to the data were the Raymond & Smith (1977) and MEKAL (Mewe et al. 1986; Kaastra 1992) codes for an optically thin thermal plasma. The column density was fixed at the Galactic value determined from radio measurements (Stark et al. 1992), and a metallicity of $0.3 Z_\odot$ was assumed. It was found that both codes gave very good agreement; the results presented here are from the MEKAL model.

Due to the very low number of counts in many of the individual cluster spectra, the spectral fits were often poorly constrained, with several not converging. In addition fits to a number of high redshift, low signal-to-noise spectra converged to low temperatures with small errors (e.g. $T=1.3 \pm 0.1$ keV). This was of concern as, according to the observed, low redshift, L - T relation, this implied luminosities too low for these clusters to be detected above the flux-limit of the survey.

There are two primary characteristics of the data which dominate the accuracy and reliability of the cluster temperature measurements, and cause the effect discussed in the previous paragraph. Firstly, the signal-to-noise of the cluster above the background, and secondly, the accuracy to which the background level can be determined. To investigate possible systematic biases caused by poor photon statistics and erroneous background estimates, extensive simulations were performed, using the ASTERIX SSIM package. Fig. 1 shows spectrally fitted temperatures from 100 datasets all simulated from a 5keV MEKAL model. Each cluster was simulated as excess emission on top of a PSPC background of 800 counts (0.1–2.3 keV, in the extraction region). This background is brighter than any found in the actual observations; hence the background level can be accurately determined in these simulations. The total number of counts is varied according to Poisson statistics. Spectral fits were performed on the emission after the background was subtracted.

It can be seen from the histogram that for the spectra (in this case with an average of ~ 190 counts in the 0.1–2.3 keV band, giving a signal-to-noise of 6.0), three distinct temperature populations were found. Spectral fits that were poorly constrained had the best-fitting temperatures pegged at a maximum value (17 keV in this case). For a different subset of spectra the fit essentially recovered the simulated temperature. However, a third population of low temperature fits with small errors was also found, as observed with some of the *ROSAT* datasets. This is a demonstration of the bias introduced with low signal-to-noise in the cluster spectra, but with the background level reasonably well determined.

The combination of the biases due to low signal-to-noise and poor background statistics, is demonstrated in Fig. 2, which shows the results from 200 simulated spectra, each containing ~ 120 counts (0.1–2.3 keV). The background level in this simulation was tailored to give a signal-to-noise values around 7 (i.e. to have ~ 175 counts, 0.1–2.3 keV). Here the individual fits cannot recover the simulated temperature of 5 keV.

A method of increasing the signal-to-noise of the spectra was thus required to enable accurate temperature estimates to be made. This was achieved via simultaneous multiple fitting of data sets in binned groups.

3.2 Multiple fitting

The effect of multiply fitting poor signal-to-noise datasets can be seen in the inset panels in both Fig. 1 and Fig. 2. These show temperatures estimated from simultaneously fitting subsets of five of the simulated datasets discussed in the previous section. In most cases, values around the simulated temperature of 5 keV were found by these fits.

As can be seen from Fig. 2, the primary effect of reducing the cluster count level, together with incorporating a low statistical accuracy background measurement, is to produce a number of simultaneous fits that are not constrained and yield the maximum allowed temperature of 17 keV. As the simulated signal-to-noise level is similar to the poorer PSPC spectra used in this work, we might expect to see this effect when using this method on WARPS clusters. No such trend was observed though. This was probably because in the real measurements a large background area was sampled in order to derive an accurate background level. This is in contrast to the simulations, where a much noisier background measurement resulted from using an area ~ 100 times smaller (as required by the SSIM program). This difference also accounts for the increased accuracy of the simulations with higher backgrounds, but similar signal-to-noise. In the analysis of PSPC data, the large area used in the estimation of the individual background level for each cluster serves to minimize the second of the two biases discussed in the previous section.

Numerous simulations were carried out to test the effectiveness of the method. Gaussian distributions in both temperature (e.g. $\pm 1 \text{ keV}$ at 90 per cent confidence) and metallicity ($\pm 0.1 Z_\odot$), around the simulated values, were included. These extended simulations also recovered a correct temperature distribution, though with a larger spread spanning around $\pm 2 \text{ keV}$. The temperature errors obtained from the fits, however, generally encompassed the distribution range.

From all the simulations, we conclude that multiple fits

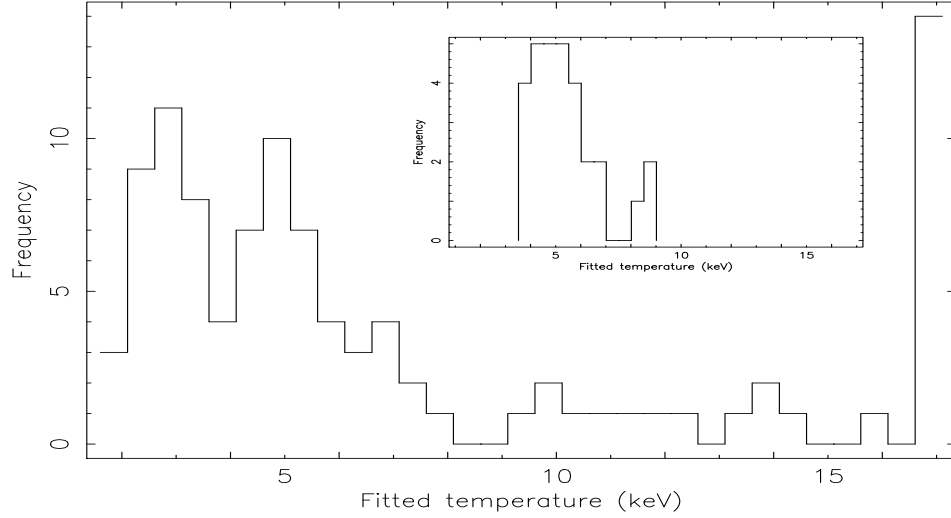


Figure 1. Spectrally fitted temperature estimates for 100 simulated 5 keV clusters with ~ 190 PSPC counts (0.1–2.3 keV). Note the three distinct populations at low temperatures, ~ 5 keV and pegged at 17 keV. Inset is the recovered temperature distribution after multiple fitting of sets of 5 such clusters.

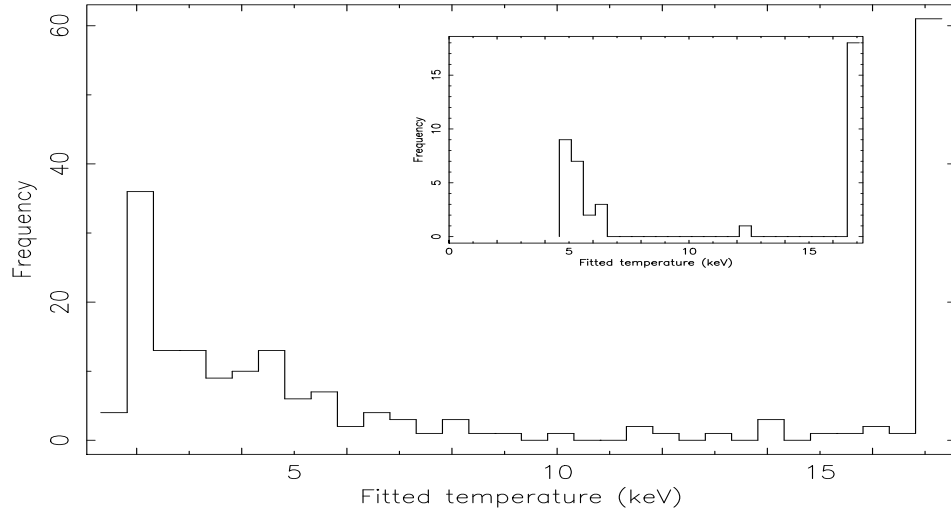


Figure 2. Spectrally fitted temperature estimates for 200 simulated 5 keV clusters with under ~ 120 PSPC counts (0.1–2.3 keV). The individual spectral fits cannot recover the simulated temperature. Inset is the recovered temperature distribution after multiple fitting of sets of 5 such clusters.

of five spectra, with each individual spectra containing 100–200 counts (i.e. a signal-to-noise ratio of 6–7 for PSPC spectra), with one free parameter, and the background statistically well determined, produce temperatures in which the level of any systematic bias is smaller than the random error. There may be an additional temperature uncertainty at

high temperatures due to PSPC calibration uncertainties. Markevitch & Vikhlinin (1997) found evidence of significant differences between PSPC and *ASCA* temperatures for $T \sim 5$ keV and higher, although the size of the differences are around the same size as our statistical error.

Multiple fitting then, was the method adopted for anal-

ysis of the PSPC spectra. In order to produce averaged spectra, we binned the clusters into redshift and luminosity bins. Where possible at least five clusters were included in each bin. Simultaneous multiple fitting was done within Version 10.0 of the XSPEC fitting package (Arnaud 1996) in the XANADU X-ray software suite. This enables several sets of data to be fitted to the same model, with certain parameters either frozen or tied to be the same for all datasets. In our case, the clusters were fitted to the same temperature in the plasma code, but with individually varying normalisations. Again, column densities were fixed at Galactic values for each cluster and metallicities were fixed at $0.3 Z_{\odot}$.

The main complication arose from the need to use maximum likelihood statistics. To correctly fit using the Cash statistic, XSPEC requires a non-background subtracted cluster spectrum, with a pre-fitted background component. Thus multiple fitting first involved individually fitting the relevant background for each cluster. The model used was an absorbed combination of a MEKAL plasma, a power law and a Gaussian emission line profile, with an initial energy of 0.54 keV (as used by Branduardi-Raymont et al. (1994) to model the X-ray background spectrum).

3.3 Luminosities

Flux estimates in the 0.5–2 keV band were obtained for each cluster from the individual fits to the spectra. These were then k-corrected, and corrected for low surface brightness emission outside the selected area assuming a King profile with $\beta = \frac{2}{3}$ and cluster core radius estimated from the VTP data, as described by Scharf et al. (1997). The fluxes were then converted to luminosities, using values of $H_0 = 50 \text{ km s}^{-1} \text{ Mpc}^{-1}$ and $q_0 = 0$. These luminosity estimates were then used for the binning of the clusters within each redshift range.

Due to the need for an accurate bolometric conversion from 0.5–2 keV luminosities, which relies on temperature estimates, the bolometric luminosities of each cluster used in the final results were obtained after the multiple fit. Each cluster was bolometrically corrected using the characteristic temperature of the bin, before again being k-corrected and convolved through a King profile correction to produce accurate luminosities. The typical bolometric correction resulted in a factor of 2–3 increase from the 0.5–2 keV luminosity. The cluster luminosities within the bin were then averaged to provide a characteristic bin luminosity.

The steep slope and large inherent scatter of the low redshift L - T relation (e.g. David et al. 1993; White et al. 1997), heightens the importance of restricting the range of luminosities within each luminosity bin. A large spread in luminosities could result in large temperature differences in the clusters contained within any bin. Which would then invalidate the simultaneous fitting method employed. The flux-limited nature of the WARPS data meant that a large spread in luminosities was found only when attempting to bin together a number of the more luminous clusters within each redshift range. In two cases, for instance, there was no other cluster of similar luminosity to the most luminous cluster, and so this cluster was individually fitted for temperature. Both WARPJ1416.4+2315 at $z = 0.137$ and WARPJ1418.5+2510 at $z = 0.294$ had more than 800 counts in the 0.1–2.3 keV band, allowing a robust temperature fit.

This also had the effect of reducing the largest spread of signal-to-noise ratios within any bin to less than a factor of two.

4 RESULTS

4.1 X-ray luminosity–temperature relations

Fig. 3 shows the L - T relation from binned PSPC spectra of WARPS clusters. Different symbols represent the redshift bins used. The luminosity errors are negligible in most cases, and primarily due to temperature uncertainties affecting the bolometric correction.

To put this L - T relation in context, Fig. 4 through Fig. 6 show the WARPS data points superposed on cluster L - T measurements drawn from the literature. Data are included from a number of different sources, including David et al. (1993), Mushotzky & Scharf (1997) and recent results from Donahue et al. (1999). The Donahue et al. (1999) dataset includes cluster measurements from a number of other works (Donahue 1996; Henry 1997; Hattori et al. 1997; Donahue et al. 1998). Data from a recent survey of 24 galaxy groups showing diffuse X-ray emission (Helsdon & Ponman 2000), are also included.

To enable us to discuss any possible evolution within the WARPS L - T relation, it is important to have a suitable low redshift relation to compare to. Mushotzky & Scharf (1997) have found no evolution in the L - T relation out to $z \sim 0.3$. So we include all clusters at $z < 0.2$ in our low redshift sample (Fig. 4). The WARPS points are in good agreement with previous measurements and help fill the gap in the L - T observations at $T=1$ –3 keV.

In order to define a fiducial low-redshift L - T relation, we obtained the best-fitting power law to the data in Fig. 4 at $T > 1$ keV. Below $T=1$ keV, there may be a systematic trend towards lower luminosities, away from the best-fitting line obtained at higher temperatures (Ponman et al. 1996; Helsdon & Ponman 2000). To allow for the systematic error intrinsic to the use of datasets from three different X-ray observatories and measured over different energy ranges, a minimum error of 5 per cent was assigned to each cluster temperature where the existing error was not already greater than this value. The best fitting slope was then found using χ^2 minimisation on the temperature axis. For $L_{\text{Bol}} = CT^{\alpha}$, we find $\alpha = 3.15 \pm 0.06$ and $C = 6.04 \pm 1.47 \times 10^{42} \text{ ergs}^{-1}$ (90 per cent confidence regions). Most previous cluster L - T relations had a best-fitting slope of around $L \propto T^{2.8 \pm 0.2}$ (e.g. Mushotzky & Scharf 1997, David et al. 1993). Our result has a slightly steeper slope primarily due to the inclusion of less luminous clusters not analysed in previous investigations.

4.2 Measuring evolution

For the purposes of constraining evolution in the normalisation of the WARPS L - T relation we assume a fixed slope of $\alpha = 3.15$ (section 4.1). We then further parametrize the L - T relation as $L_{\text{Bol}} = C(1+z)^{\eta}T^{\alpha}$ where $C = 6.04 \times 10^{42} \text{ ergs}^{-1}$, the best-fitting normalisation of the local L - T relation. The η term then parametrizes evolution at any redshift z .

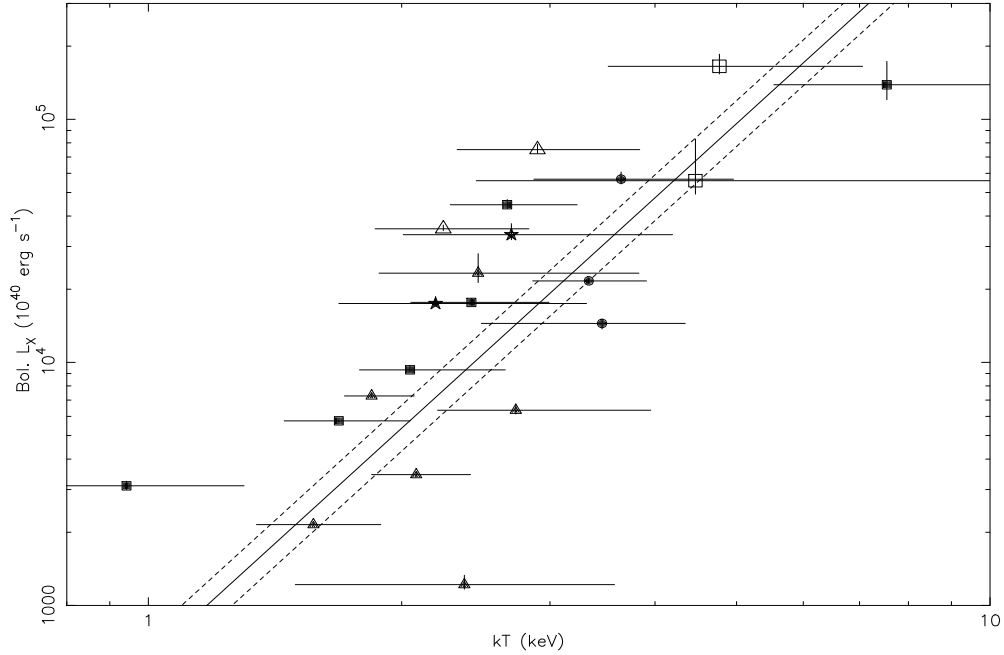


Figure 3. The L–T relation from binned PSPC spectra of WARPS clusters. Filled triangles represent clusters in the $0.1 < z < 0.2$ bins. Filled squares represent $0.2 < z < 0.3$, circles $0.3 < z < 0.4$, stars $0.4 < z < 0.5$, open triangles $0.5 < z < 0.6$ and open squares clusters of $z > 0.6$. Each point is shown with 1σ temperature and luminosity errors. Also shown is the best-fitting line to the data shown in figure 4 at $T > 1$ keV, $L \propto T^{3.15}$ with its 90 per cent confidence normalisation errors.

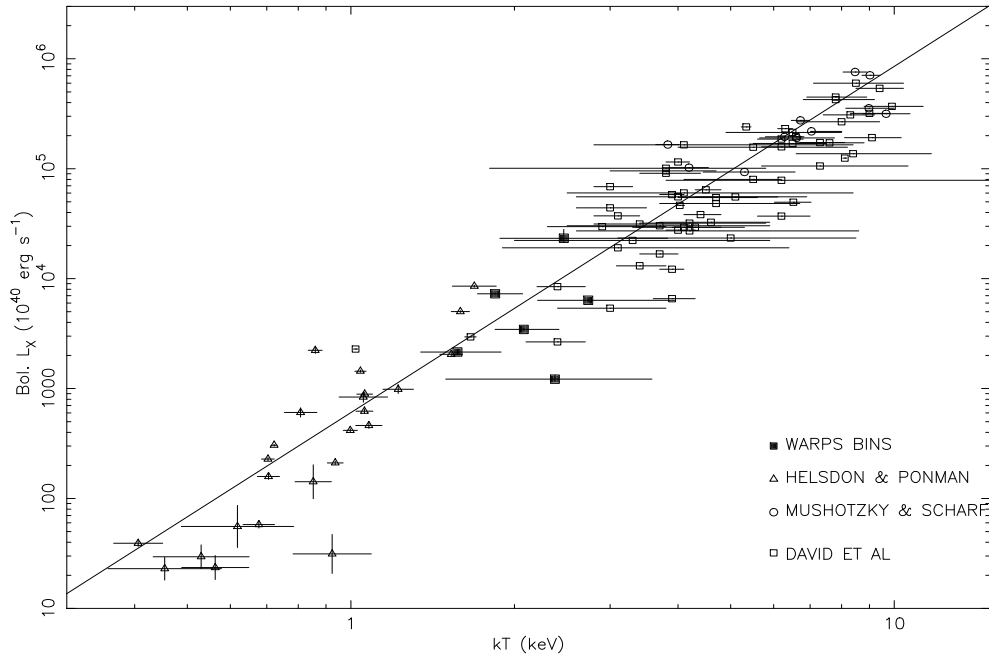


Figure 4. L–T relation for $z < 0.2$. Triangles represent groups from Helsdon & Ponman (2000), filled squares are WARPS bins, open circles are clusters from Mushotzky & Scharf (1997) and open squares are clusters from David et al. (1993). The line shown is the best-fitting line to clusters with $T > 1$ keV, $L \propto T^{3.15}$.

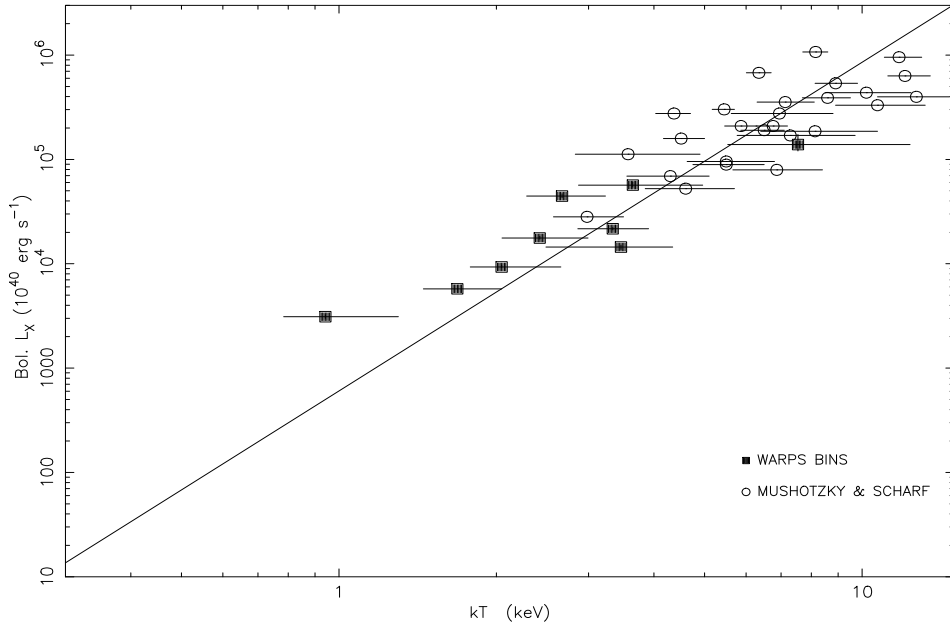


Figure 5. L - T relation for $0.2 < z < 0.4$. Filled squares represent WARPS bins, open circles are clusters from Mushotzky & Scharf (1997). The line shown is the best-fitting line from the $z < 0.2$ sample.

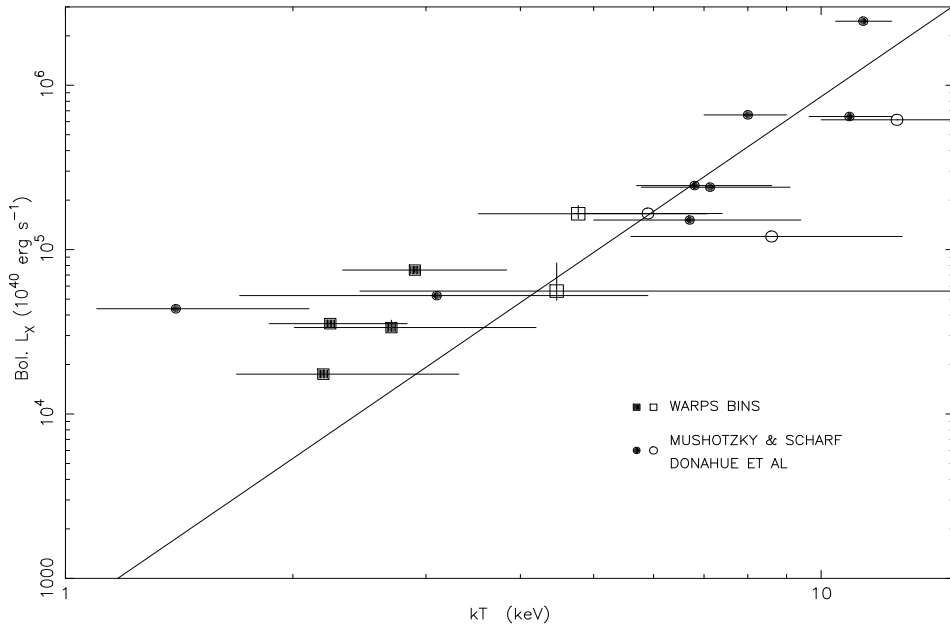


Figure 6. L - T relation for $0.4 < z < 0.6$ and $z > 0.6$. Squares represent WARPS bins, circles are clusters from Mushotzky & Scharf (1997) and recent results from Donahue et al. (1999). In both cases solid points represent datapoints from the $0.4 < z < 0.6$ range, and open points $z > 0.6$. The line shown is the best-fitting line from the $z < 0.2$ sample.

We now consider the WARPS measurements in the redshift ranges shown in Fig. 5 and Fig. 6. Assuming the best-fitting slope from the low redshift clusters, we again fit for normalisation by minimising the χ^2 -statistic. Again only measurements above 1 keV were included in the fit. Taking the central redshift of these bins allows us to evaluate η and

its associated error. Most theoretical studies discuss evolution in the L - T relation in terms of an $\Omega_0 = 1$ cosmology. Table 1 displays our evolutionary constraints (η values) found for the three $z > 0.2$ redshift ranges assuming $\Omega_0 = 1$. Whenever a different cosmology is specified, we corrected cluster

Table 1. η values for WARPS bins and WARPS bins combined with Mushotzky & Scharf (1997) and Donahue et al. (1999) measurements, assuming an $\Omega_0 = 1$ cosmology. Errors shown are 1σ . A weighted average is also given.

z range	WARPS η values	All data η values
0.2–0.4	0.82 ± 1.01	0.87 ± 0.55
0.4–0.6	2.64 ± 1.12	0.56 ± 0.52
0.6+	0.45 ± 1.99	-1.46 ± 0.86
Average=	1.42 ± 0.83	0.19 ± 0.38

luminosities accordingly (we assume $H_0 = 50 \text{ km s}^{-1} \text{ Mpc}^{-1}$ throughout).

In order to further constrain evolution in the L–T plot, the number of data points in each redshift bin must be increased. Using datasets from Mushotzky & Scharf (1997) and Donahue et al. (1999) in conjunction with the WARPS bins, we were able to place tighter constraints on evolution in the L–T plot. The data used are represented in Figs 5 and 6, and the resulting η values are listed in Table 1.

It can be seen from Table 1 that in general the WARPS measurements are consistent with no evolution of the normalisation of the L–T relation (though one redshift range provides marginal evidence for evolution). When the WARPS points are combined with other existing cluster measurements the results are also consistent with no evolution. To quantify the level of evolution measured we give the averaged η value of the three separate redshift range measurements. The averages have been weighted by the inverse errors. The averaged η value of the combined dataset for $\Omega_0 = 1$ ($\eta = 0.19 \pm 0.38$), is consistent with no evolution to $z \sim 0.8$. Changing the cosmology used in the fit to an open $\Omega_0 = 0.3$, $\lambda_0 = 0$ Universe modifies the conclusion only slightly, producing $\eta = 0.60 \pm 0.38$, still consistent with no evolution at around the 1.5σ level.

5 DISCUSSION

5.1 Theoretical relations

The implications of the evolution parameter, η , can now be discussed in terms of evolution of X-ray temperatures and luminosities in the L–T relation. Here we focus primarily on comparisons with the entropy driven evolution model of Bower (1997) and its extension to various cosmologies (Kay & Bower 1999). In this model the evolution of the X-ray properties of clusters is split into contributions from the gravitational heating of the ICM and from purely gas related processes, such as shock heating or radiative cooling. Assuming a minimum entropy (or entropy floor) in cluster cores allows deviations from the pure self-similar scaling of the cluster ICM with the underlying dark matter distribution (e.g. Kaiser 1991; Evrard & Henry 1991). The entropy driven model further allows the exploration of the regime between the purely self-similar scaling predictions of Kaiser (1986) and the effect of a pre-heated ICM.

As discussed by Bower (1997), the heating and cooling of the ICM gas can be described in terms of evolution of the core entropy, if we assume that the slope of the primordial density fluctuation power spectrum, n , controls the gravita-

tional growth of clusters. Parameterizing this evolution in the form $s_{\text{min}} = s_{\text{min}}(z = 0) + c_v \epsilon \ln(1 + z)$ describes the level of the entropy floor, s_{min} , at any redshift, z . The term ϵ thus describes how this entropy evolves (c_v is just the specific heat capacity of the gas at constant volume). A negative value represents continual shock heating of the ICM during cluster collapse and $\epsilon > 0$ describes a cluster core dominated by radiative cooling, whilst $\epsilon = 0$ is the constant entropy model (e.g. Evrard & Henry 1991). It is then possible to derive a functional form for the L–T relation, with evolution of its normalisation parametrized in terms of n , and ϵ . If we assume the density profile parameter is equal to the canonical value of, $\beta = 2/3$, then both the Bower (1997) and Kay & Bower (1999) scaling relation models give an L–T relation of the form $L_{\text{Bol}} \propto (1 + z)^{-3\epsilon/4} T^{2.75}$. Although we find a slightly different value of the slope of the L–T relation than this, due to the assumption of weak self-similarity (section 2.4, Bower (1997)), we are only concerned with the evolution of normalisation of the relation. We therefore use a fixed slope of $L_{\text{Bol}} \propto T^{3.15}$ when dealing with these scaling relations. The main effect of the difference in slope is to introduce a slight degeneracy between n and ϵ when calculating the expected normalisation of the L–T relation (e.g. fig. 2, Bower 1997).

We can use the scaling relations to predict the evolution in normalisation of the L–T relation in terms of n and ϵ . An example is shown in Fig. 7. Here we have assumed a temperature scaling relation as in Equation 2.11 of Kay & Bower (1999). Assuming an underlying cosmology ($\Omega_0 = 0.3$, $\lambda_0 = 0$ in this case) and a value of the initial power spectrum (here $n = -1.6$, in agreement with the measured APM galaxy power spectrum, Tadros et al. 1998), we can use the lack of observed evolution in the L–T relation to constrain evolution in the cluster core entropy. This evolution of the entropy floor is represented by the expected normalisation of the L–T relation changing, with redshift, as a function of the value of ϵ , as shown in Fig. 7. Here the degeneracy with n is introduced in the calculation of Equation 2.11 of Kay & Bower (1999) and also with the effect of a changing epoch of cluster formation as in Equations 2.12 and 2.13. The lack of observed evolution (as demonstrated by the value of the η parameter being consistent with zero), implies almost no evolution of cluster core entropy to $z \sim 0.8$ given the assumed cosmology and value of n . Table 2 details our calculated ϵ values in both an open and closed cosmology, for three different n values. Also tabulated are the corresponding values required for pure self-similar scaling in an $\Omega_0 = 1$ cosmology (Kaiser 1986), given by $\epsilon_{\text{ss}} = -\frac{(n+7)}{(n+3)}$, which is strongly ruled out.

So far we have not attempted to place any cosmological constraints. To do this we need to break the degeneracy that allows evolution in the X-ray properties to be explained via either gravitational or gas-phase phenomena. This requires the introduction of a second dataset. The XLF, for instance, allows the values of n and ϵ to be constrained in an almost orthogonal manner to the L–T evolution constraints. This is demonstrated in fig. 3 of Kay & Bower (1999). If the XLF is non-evolving to high redshift, as several recent studies have found (Burke et al. 1997; Jones et al. 1998b; Rosati et al. 1998; Ebeling et al. 2000), then important constraints can be placed on the underlying cosmology. Given that the value of ϵ is more tightly constrained in this work than in

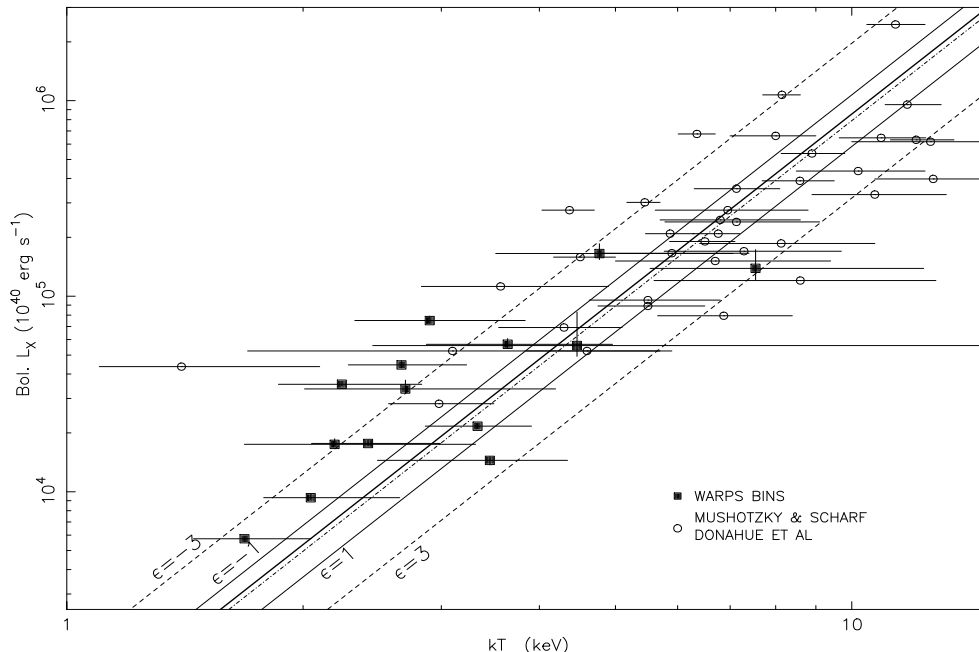


Figure 7. The L - T relation data above $z = 0.2$, with normalisation predictions from Kay & Bower (1999). WARPS points are shown as solid squares and the combined data of Mushotzky & Scharf (1997) and Donahue et al. (1999) are displayed as open circles. The thick line represents the low redshift best-fitting relation. Plotted on the graph are predictions of the normalisation of the L - T relation assuming $\Omega_0 = 0.3$ and $n = -1.6$. Lines are calculated for a redshift of $z = 0.5$, assuming 5 different values of ϵ . The dot-dashed line represents $\epsilon = 0$, the thin solid lines $\epsilon = 1$ and $\epsilon = -1$, and the dashed lines $\epsilon = 3$ and $\epsilon = -3$. For illustrative purposes the lines have been converted back to a $q_0 = 0$ cosmology, to match the datapoints displayed in Fig. 3 through Fig. 6.

Table 2. Constraints on the entropy evolution of cluster cores, as represented by the ϵ parameter. Values are listed for 3 different values of the primordial fluctuation power spectrum, n , and in two different cosmologies. ϵ values predicted for pure self-similar scaling (Kaiser 1986) are also given.

n value	$\epsilon \pm 0.51(1\sigma)$ $\Omega_0 = 0.3, \lambda_0 = 0$	$\epsilon \pm 0.51(1\sigma)$ $\Omega_0 = 1$	ϵ (self-similar) $\Omega_0 = 1$
-1	-0.76	0.28	-3.00
-1.6	-0.55	0.74	-3.86
-2	-0.26	1.35	-5.00

Kay & Bower (1999), any fluctuation spectrum of $n < -1.5$ requires a Universe with a low value of Ω_0 ($\Omega_0 < 0.5$). Correspondingly, values of $n \sim -1$ are required to be consistent with the observed XLF and L - T relation evolutionary constraints in an $\Omega_0 = 1$ universe. Allowing for the possibility of some negative evolution in the XLF at the highest luminosities, as some surveys find (Henry et al. 1992, Vikhlinin et al. 1998a), may relax these constraints slightly, although the evolution at these high luminosities is not observationally well determined.

5.2 Cooling flows

The abundance of cooling flows within the WARPS cluster survey could have a large effect on the estimated clus-

ter luminosity-temperature relation. Allen & Fabian (1998) showed that when the most X-ray luminous clusters were modelled isothermally, non-cooling flow clusters had significantly higher temperatures than cooling flow clusters. Furthermore, they found a significant change in the best-fitting slope of the cluster L - T relation when cooling flow clusters were analysed with an isothermal model, as opposed to a model with a central cooling flow component. They claimed a change in slope from $L \propto T^3$ to approximately $L \propto T^2$ when cooling flows were taken into account.

Due to the low signal-to-noise of the *ROSAT* X-ray data used in this work, fitting the data for a cooling flow component is not possible. However, we were able to estimate the fraction of clusters in our sample that exhibit evidence for a cooling flow. It has been shown that most clusters (≥ 70 per cent) have or can form cooling flows (e.g. Edge et al. 1992; Peres et al. 1998), though the cooling flow size is proportional to the X-ray luminosity. Some cooling flows also exhibit other characteristics, most notably optical line emission from the BCGs. The fraction of clusters in X-ray flux limited surveys displaying these properties is around 33 per cent (e.g. Edge et al. 1992; Donahue et al. 1992), though this fraction is highly dependent on the quality of the optical spectra. Less than this level of cooling flow activity in the WARPS sample would be a good indication that our survey does not over-sample cooling flows.

The optical spectra obtained to measure galaxy redshifts allowed analysis of line emission in the BCG of each cluster. In a preliminary analysis, $H\alpha$ or $[\text{OII}]\lambda 3727$ emission

lines were detected in 4 of the 26 BCG spectra analysed. This implies a fraction of 16 per cent cooling flow clusters in our survey. This might be expected if the frequency of cooling flows exhibiting optical emission lines increased in more X-ray luminous systems.

Cooling flows would produce a lower temperature estimate for the same X-ray luminosity, thus they would, in effect, mimic evolution in the WARPS results in the direction predicted for $\Omega_0 = 1$, assuming no core entropy evolution (Bower 1997). Removal of the effects of a fraction of the sample containing cooling flows would hence favour lower values of Ω_0 , strengthening our conclusion.

6 CONCLUSIONS

We have presented a cluster X-ray luminosity–temperature relation out to high redshifts ($z \sim 0.8$), based on *ROSAT* PSPC spectra of WARPS clusters. Due to the low signal-to-noise of many of our *ROSAT* PSPC spectra, a multiple fitting technique was adopted in order to constrain temperatures. The 91 clusters analysed were binned into redshift and luminosity bins, and spectrally fit to a characteristic temperature.

In order to analyse the evolution of the L–T relation, a large sample of low redshift ($z < 0.2$) clusters was compiled from the literature. The best-fitting power law to the data at low redshift and at $T > 1$ keV was found to be a power law of index $L \propto T^{3.15 \pm 0.06}$ (90 per cent confidence). This relation was then compared with the high redshift measurements to constrain possible evolution in the normalisation of the L–T relation.

The binned *ROSAT* measurements of WARPS clusters were consistent with no evolution of the L–T relation to $z \sim 0.8$. When combined with previous cluster measurements from the literature they agree with the no evolution result of Donahue et al. (1999), but give stronger constraints; $\eta = 0.19 \pm 0.38$ for $\Omega_0 = 1$, or $\eta = 0.60 \pm 0.38$ for $\Omega_0 = 0.3$ where $L_{\text{Bol}} \propto (1+z)^\eta T^{3.15}$. Using the entropy driven evolution model of Bower (1997) and Kay & Bower (1999), a limit to the implied entropy evolution of cluster cores was found. Whilst the level of entropy evolution is slightly dependent on the value of the primordial density fluctuation spectrum, n , low amounts of evolution were favoured. The pure self-similar scaling expectations of Kaiser (1986) were found to be strongly excluded.

The lack of evolution in the WARPS L–T relation, in conjunction with other recent results, such as a non-evolving XLF, implies either an open cosmology ($\Omega_0 < 1$) or one closed by a cosmological constant, assuming $n < -1$. The forthcoming X-ray missions Chandra and XMM will allow more accurate temperature estimates of clusters, out to high redshifts, which will greatly improve our understanding of the L–T relation and its cosmological implications.

7 ACKNOWLEDGMENTS

The authors would like to thank Megan Donahue and collaborators for advance access to their cluster measurements. Thanks to Scott Kay for help with the entropy evolution model. We thank the Birmingham galaxies and cluster group

for useful discussions and input. The data used in this work have been obtained from the Leicester database and archive service (LEDAS). Computing facilities provided by the STARLINK project have been used in this work. BWF acknowledges the receipt of a PPARC studentship and LRJ also acknowledges the support of PPARC. HE acknowledges financial support from SAO contract SV4-64008 and NASA LTSA grant NAG 5-8253.

REFERENCES

- Allan D. J., Vallance R. J., 1995, Starlink User Note, 98.6
- Allen S. W., Fabian A. C., 1998, MNRAS, 297, L57
- Arnaud K. A., 1996, ASP Conf. Series, 101, 17
- Bower R. G., 1997, MNRAS, 288, 355
- Branduardi-Raymont G. et al., 1994, MNRAS, 270, 947
- Burke D. J., Collins C. A., Sharples R. M., Romer A. K., Holden B. P., Nichol R. C., 1997, ApJ, 488, L83
- Cash W., 1979, ApJ, 228, 939
- Castander F. J. et al., 1995, Nature, 377, 39
- Cen R., Ostriker J. P., 1994, ApJ, 429, 4
- Collins C. A., Burke D. J., Romer A. K., Sharples R. M., Nichol R. C., 1997, ApJ, 479, L117
- David L. P., Slyz A., Jones C., Forman W., Vrtilik S. D., Arnaud K. A., 1993, ApJ, 412, 479
- De Grandi S. et al., 1999, ApJ, 513, L17
- Donahue M., 1996, ApJ, 468, 79
- Donahue M., Stocke J. T., Gioia I. M., 1992, ApJ, 385, 49
- Donahue M., Voit G. M., Gioia I., Luppino G., Hughes J. P., Stocke J. T., 1998, ApJ, 502, 550
- Donahue M., Voit G. M., Scharf C. A., Gioia I. M., Mullis C. R., Hughes J. P., Stocke J. T., 1999, ApJ, 527, 525
- Ebeling H., Wiedenmann G., 1993, Phys. Rev., 47, 704
- Ebeling H., Edge A. C., Fabian A. C., Allen S. W., Crawford C. S., Bohringer H., 1997, ApJ, 479, L101
- Ebeling H. et al., 2000, ApJ, in press
- Edge A. C., Stewart G. C., 1991, MNRAS, 252, 414
- Edge A. C., Stewart G. C., Fabian A. C., 1992, MNRAS, 258, 177
- Evrard A. E., Henry J. P., 1991, ApJ, 383, 95
- Frenk C. S., White S. D. M., Efstathiou G., Davis M., 1990, ApJ, 351, 10

- Gioia I. M., Henry J. P., Maccacaro T., Morris S. L., Stocke J. T., Wolter A., 1990, *ApJ*, 356, L35
- Hattori M. et al., 1997, *Nature*, 388, 146
- Helsdon S. F., Ponman T. J., 2000, *MNRAS*, in press
- Henry J. P., 1997, *ApJ*, 489, L1
- Henry J. P., Gioia I. M., Maccacaro T., Morris S. L., Stocke J. T., 1992, *ApJ*, 386, 408
- Henry J. P., Jiao L., Gioia I. M., 1994, *ApJ*, 432, 49
- Jones L. R., Scharf C., Ebeling H., Perlman E., Wegner G., Malkan M., Horner D., 1998a, *ApJ*, 495, 100
- Jones L. R., Scharf C., Perlman E., Ebeling H., Horner D., Wegner G., Malkan M., McHardy I., 1998b, *Astron. Nachr.*, 319, 87
- Kaastra J. S., 1992, Internal SRON-Leiden Report, Updated version 2.0
- Kaiser N., 1986, *MNRAS*, 222, 323
- Kaiser N., 1991, *ApJ*, 383, 104
- Kay S. T., Bower R. G., 1999, *MNRAS*, 308, 664
- Lucey J. R., 1983, *MNRAS*, 204, 33
- Markevitch M., Vikhlinin A., 1997, *ApJ*, 474, 84
- Mewe R., Lemen J. R., van den Oord G. H. J., 1986, *A&A*, 65, 511
- Mushotzky R. F., Scharf C. A., 1997, *ApJ*, 482, L13
- Nousek J. A., Shue D. R., 1989, *ApJ*, 342, 1207
- Peres C. B., Fabian A. C., Edge A. C., Allen S. W., Johnstone R. M., White D. A., 1998, *MNRAS*, 298, 416
- Perlman E., Horner D., Jones L. R., Scharf C., Ebeling H., Wegner G., Malkan M., 2000, in preparation
- Ponman T. J., Bourner P. D. J., Ebeling H., Bohringer H., 1996, *MNRAS*, 283, 690
- Raymond J. C., Smith B. W., 1977, *ApJS*, 35, 419
- Romer A. K. et al., 2000, *ApJS*, in press
- Rosati P., Della Ceca R., Burg R., Norman C., Giacconi R., 1995, *ApJ*, 445, L11
- Rosati P., Della Ceca R., Norman C., Giacconi R., 1998, *ApJ*, 492, L21
- Scharf C., Jones L. R., Ebeling H., Perlman E., Malkan M., Wegner G., 1997, *ApJ*, 477, 79
- Stark A. A., Gammie C. F., Wilson R. W., Bally J., Linke R. A., Heiles C., Hurwitz M., 1992, *ApJS*, 79, 77
- Struble M. F., Rood H. J., 1991, *ApJ*, 374, 395
- Tadros H., Efstathiou G., Dalton G., 1998, *MNRAS*, 296, 995
- Vikhlinin A., McNamara B. R., Forman W., Jones C., Quintana H., Hornstrup A., 1998a, *ApJ*, 498, L21
- Vikhlinin A., McNamara B. R., Forman W., Jones C., Quintana H., Hornstrup A., 1998b, *ApJ*, 502, 558
- White D. A., Jones C., Forman W., 1997, *MNRAS*, 292, 419